NOTE
DE CENTRE

N° 33

A subgrid convection scheme for representing dry, moist and precipitating convection in large-scale models, PCMT. II: one-and three-dimensional evaluation

J.-F. Guérémy, J.-M. Piriou, J. Colin, I. Beau, D. Saint-Martin, F. Bouyssel, R. Roehrig, E. Bazile, J.-P. Lafore and D. Pollack

Novembre 2018

CENTRE NATIONAL
DE RECHERCHES MÉTÉOROLOGIQUES

A subgrid convection scheme for representing dry, moist and precipitating convection in large-scale models, PCMT. II: one- and three-dimensional evaluation

J.-F. Guérémy,[a*] J.-M. Piriou,[a] J. Colin,[a] I. Beau,[b] D. Saint-Martin,[a]
F. Bouyssel,[a] R. Roehrig,[a] E. Bazile, [a]J.-P. Lafore[a] and D. Pollack[b]

[a]*Météo-France, Centre National de Recherches Météorologiques (CNRM), Toulouse, France*
[b]*Météo-France, École Nationale de la Météorologie (ENM), Toulouse, France*

[*]Correspondence to: J.-F. Guérémy, Météo-France, Centre National de Recherches Météorologiques (CNRM), 42 av. G. Coriolis, 31057 Toulouse, France
E-mail: jean-francois.gueremy@meteo.fr

Abstract

A new convection scheme evaluation and sensitivity is described. First, single column model (SCM) simulations of three representative convective cases are analyzed to assess the scheme response. Among the small number of the scheme parameters, two of them are selected to investigate the scheme sensitivity throughout the article, the maximum value of the turbulent entrainment rate and the solid auto-conversion rate. A relevant SCM simulation shows that an entrainment decrease favours moderate at the expense of shallow convection tending to moisten the troposphere, whereas a solid auto-conversion increase tends to dry the troposphere due to a decrease of stratiform precipitation evaporation induced by a smaller detraining convective condensate. Two other independent cases, continental and maritime diurnal cycles, show a proper behaviour of the convection scheme and a significant sensitivity to the entrainment decrease for the former. Second, general circulation model simulations are evaluated in terms of mean climate, intraseasonal (diurnal cycle, distribution of daily precipitation and outgoing long-wave radiation intraseasonal variability) and interannual variability. The reference simulation shows a rather good skill in reproducing these four items. Decreasing the entrainment rate provokes a tropospheric moistening (as for the SCM simulation), a negative 2-hour shift in the diurnal cycle, a tightening of the precipitation distribution and a scale broadening of both intraseasonal and interannual response to convection. Increasing the solid auto-conversion results in a tropospheric drying (as for the SCM simulation), a slight increase of moderate precipitation and a narrowing of both intraseasonal and interannual response to convection.
Key words: convection scheme; model evaluation; entrainment rate; precipitation efficiency; diurnal cycle; distribution of precipitation; tropical intraseasonal variability; seasonal teleconnections.

1. Introduction

The convection scheme is a key element of large-scale models. It is designed to represent processes occurring at scales smaller than those of the processes resolved by these large-scale models. Furthermore, the subgrid-scale processes parametrised by this scheme, together with the turbulence scheme, constitute the basis of the atmospheric response to the radiative forcing. These processes include both transport and water phase changes.

Such convection schemes have been developed since the beginning of large-scale modelling (Arakawa, 2004). Most of the present convection schemes use a mass flux concept (e.g. Bougeault, 1985; Tiedtke, 1989; Gregory and Rowntree, 1990; Kain and Fritsh, 1990; Emanuel, 1991; Zhang and McFarlane, 1995). Recent efforts have been made at Météo-France to design a new convection scheme called Prognostic Condensates Microphysics and Transport (PCMT) taking advantage of previous works (Piriou et al., 2007; Guérémy, 2011). This new scheme has been implemented in the Météo-France general-circulation model (GCM) called ARPEGE, and more specifically for the present article in ARPEGE-Climat used in climate research (Voldoire *et al.*, 2013). Together with PCMT, two other new schemes have been implemented in this model to go from the version 5 described in the previous reference to the new version 6 used here: a turbulence scheme following the approach of Cuxart et al. (2000) which represents the TKE with a 1.5-order prognostic equation allowing the computation of both stratiform cloudiness and water content in a consistent way, according to Sommeria and Deardorff (1977), and a microphysics scheme following the work of Lopez (2002) which takes into account the processes of autoconversion, sedimendation, icing-melting, precipitation evaporation and collection. This model can be used either in a single-column model (SCM) mode or in a GCM mode.

PCMT provides a continuous, consistent, and prognostic treatment of convection from dry thermals to deep precipitating events. The continuity of modelled convection is not common among other parametrisations, where, for example, a distinct treatment is carried out for shallow and deep convection (Tiedtke, 1989; Gregory and Rowntree, 1990). PCMT proposes a continuous formulation of both cloud profile (including entrainment-detrainment) and closure condition, with a convective updraught possibly starting from dry thermals. The scheme consistency is ensured by the use of the buoyancy in the definition of the cloud profile and the closure condition. The convective vertical velocity is prognostic (buoyancy as the main source term), while being central in the cloud profile (triggering, entrainment-detrainment rates, normalized convective fraction along the vertical, and mass flux). Convective tendencies are directly expressed in terms of transport and condensation following Piriou *et al.* (2007). Condensation tendency is entering into the same microphysics scheme as for stratiform processes (Lopez, 2002) giving rise to prognostic convective water contents. Finally, as a result of its continuous and consistent character, PCMT presents a small number of parameters to be tuned. An extensive description of PCMT is provided in Part I of this paper by Piriou and Guérémy (2018).

The aim of this article is to describe an evaluation and sensitivity study of PCMT convection scheme. Single Column Model (SCM) validation, using well documented case studies based on field campaigns, is the first necessary step to fulfill in any scheme assessment. This has been widely used by previous authors (e.g. Tiedtke, 1989; Gregory and Rowntree, 1990; Bechtold *et al.*, 2001;

Bretherton *et al.*, 2004). Moreover, SCM validation was the main methodology applied in the framework of the European Cloud Systems Project (EUROCS) (Grabowski and Kershaw, 2004). SCM simulations carried out in a prognostic mode, taking into account the evolution of temperature, water and momentum (Betts and Miller, 1986), are crucial in order to assess the one-dimensional response of convection in such constrained environments. Making use of several representative convective cases, including explicit simulations such as Large Eddy Simulations (LES) (e.g. Siebesma *et al.*, 2003) or Cloud Resolving Model (CRM) simulations (e.g. Bechtold *et al.*, 2000), allows a careful tuning of the parametrisation. Nevertheless, SCM validation is obviously insufficient, due to the absence of feedback between the simulated column and its initially nearby neighbors. This is the reason why three-dimensional simulations are the second necessary step to perform in a new scheme evaluation process. Many previous studies have conducted such simulations, mainly using General Circulation Models (GCMs), concentrating in the mean climate evaluation (e.g. Tiedtke, 1989; Zhang and McFarlane, 1995). More recently, some authors have investigated the ability of new or improved convection schemes to accurately reproduce the climate variability and predictability (e.g. Bechtold *et al.*, 2008; Bechtold *et al.*, 2014; Klingaman *et al.* 2015). An interesting and fruitful intermediate step between SCM case study and GCM simulations has been applied at Météo-France, consisting in an evaluation of a three-dimensional limited area simulation of a field campaign case study against observations and CRM simulation (Leger, supervised by Guérémy *et al.*, 2015).

The outline of this article is as follows. Section 2 is devoted to SCM simulations. Beyond the selection of the scheme three main parameters carried out in Part I of this paper (Piriou and Guérémy, 2018) making use of three representative SCM convective case studies, two parameters, the turbulent entrainment and the solid auto-conversion rates are considered all along the present article to perform sensitivity experiments. Moreover, two additional convective case studies are simulated in order to evaluate the scheme in SCM mode. The three-dimensional sensitivity and evaluation results are presented in Section 3. They include both mean climate and intraseasonal to interannual variability aspects.

2. SCM evaluation

The scheme evaluation is carried out in a SCM mode framework using ARPEGE-Climat (with 91 vertical levels, from 10 m up to 80 km above ground, 14 levels being below 1500 m), on two selected case studies, representative of diurnal cycle of convection over both continent and ocean. The main goal of this evaluation is to ensure the relevance of the parameter choice undertaken in Part I. In between those two steps, an intermediate one has been devised to define 2 parameters among those providing the most sensitive response of the scheme: the turbulent entrainment rate (its maximum value, see section 3 of Part I) and the precipitation efficiency (the solid auto-conversion rate, see section 4 of Part I). Two sensitivity experiments result from this choice. The analysis of these two experiments will be discussed throughout the evaluation process, from and beyond the SCM mode framework.

2.1 Scheme sensitivity

As previously mentioned, the maximum turbulent entrainment rate and the solid auto-conversion rate are considered in order to define two sensitivity experiments, respectively called SEt and SEp, to be compared to the control experiment called REF. SEt, the experiment with less entrainment, is conducted using the nominal Etx parameter minus 56% (i.e. $4 \times 10^{-5} Pa^{-1}$), and SEp, the experiment with a larger precipitation efficiency, is conducted using the nominal ACs parameter plus 57% (i.e. $55 \times 10^{-4} s^{-1}$).

The Derbyshire *et al.* (2004) case study (hereafter called D04, designed to investigate the sensitivity of moist convection to environmental humidity) enables a relevant illustration of the scheme sensitivity considering the two extreme relative humidity values: RH25 (i.e. the non precipitating shallow convection case) and RH90 (i.e. the precipitating deep convection case). Figures 1(a)-(f) show the time evolution of the simulated cloud fraction over a 24 h period, of the RH25 case for REF, SEt and SEp respectively, and of the RH90 case for the same 3 experiments. These Figures 1(a)-(f) provide a first look at the sensitivity of the convective scheme to changes in the strength of entrainment and precipitation efficiency. As expected, taking into account the results obtained with the BOMEX case study in Part I, it appears clearly that reducing Etx (SEt experiment) triggers a deepening of convection seen both for RH25 and RH90. Whereas, increasing the precipitation efficiency (SEp experiment) tends to contract the convection both for RH25 and RH90; but the magnitude of change is less than for SEt.

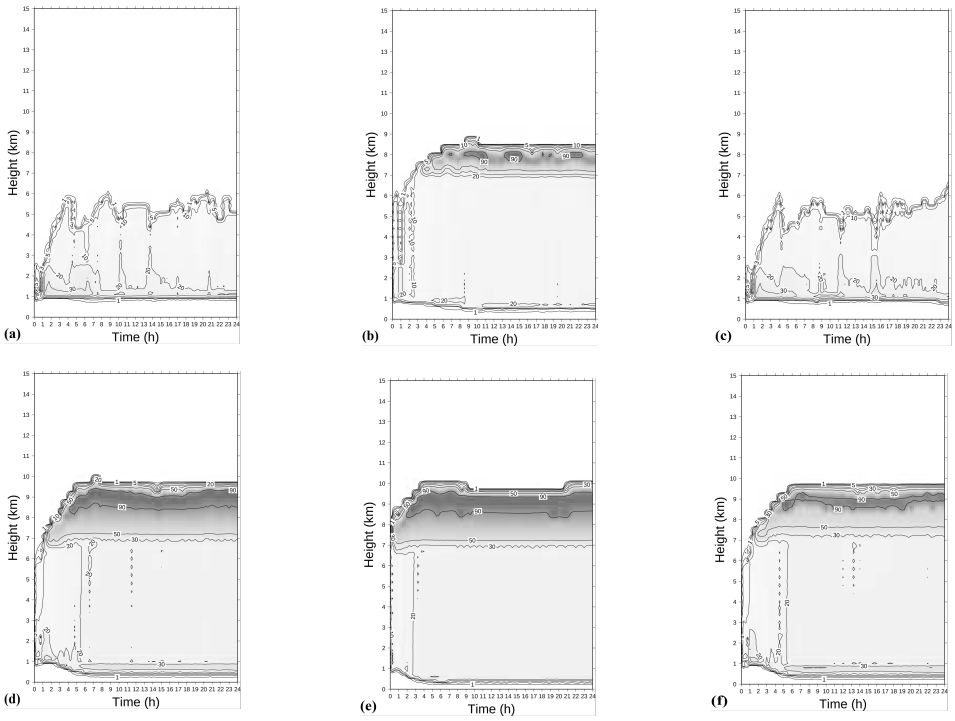

Figure 1. Derbyshire *et al.* (2004) case. Time evolution of the SCM cloud fraction (%) for the RH25 case (a) REF, (b) SEt, (c) SEp, and for the RH90 case (d) REF, (e) SEt, (f) SEp.

The apparent moisture sink (Q2) profiles of the simulations RH25 and RH90, for the three experiments, are depicted in Figures 2(a) and (b) respectively. They enables to understand the physical reason of the response, especially concerning the SEp experiment. Indeed, the impact of a decrease of entrainment (SEt experiment) on Q2 is quite clear, as a consequence of the convective deepening, i.e. a drying below 5000 m and a moistening above, by comparison to REF. The latter effect tends to further enhance the response in the same direction (positive feedback), the moister the environment the deeper the convection. Here, the results are the same as in Wang *et al.* (2007), i.e. dipole drying-moistening when the shallow convection entrainment rate is decreased (see their Figure 9 (g)). Concerning the SEp experiment, a slightly weaker moistening appears in the upper part of the Q2 profiles. This is due to the fact that the convective solid condensate, being more rapidly transformed into convective solid precipitation (just slightly evaporated due to the convective saturated environment), will be evaporated in a smaller quantity after being detrained into stratiform solid condensate (see the microphysics described in Part I). This drying trend will then reinforce the less intense convection.

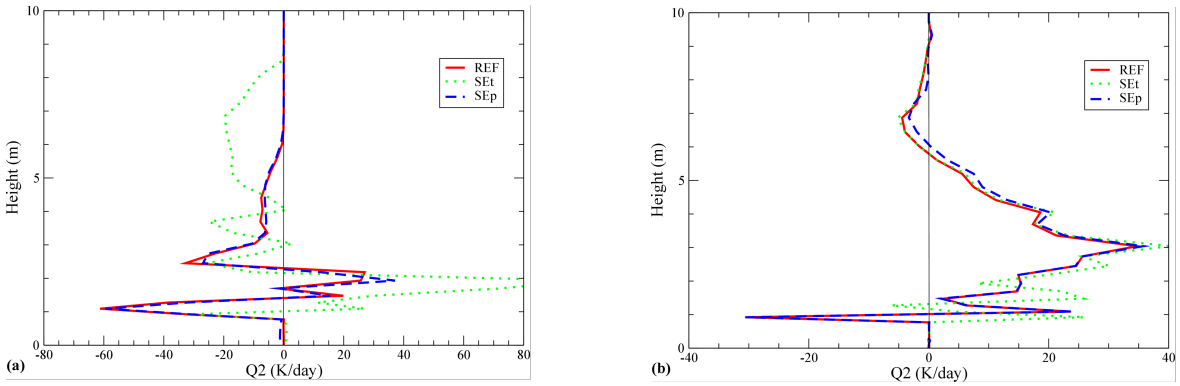

Figure 2. Derbyshire *et al.* (2004) case. Apparent moisture sink over the quasi-steady period of REF, SEt and SEp for (a) the RH25 case and (b) the RH90 case.

2.2 Scheme evaluation

2.2.1 Diurnal cycle of continental convection

The considered case study has been set-up by Guichard *et al.* (2004), hereafter called G04, in order to investigate the ability of SCM simulations to reproduce an entire continental diurnal cycle of convection, from the convective dry layer build-up to the precipitating deep convection stage. The main forcings of this case study are the surface heat fluxes provided every 30 mn in order to obtain a precise diurnal evolution. The sensible heat flux reaches 120 Wm^{-2} at around 11 h (local time), and the latent heat flux rises to 400 Wm^{-2} one hour later (as depicted in Figure 1 of G04).

Figures 3(a) and (b) (REF and SEt experiments respectively) show the time evolution of the simulated cloud fraction over a 21 h period, covering the convective diurnal evolution. For the REF experiment, the first shallow cumulus clouds appear at around 1000 h (local time), i.e. 1 h before what is simulated with the CNRM CRM, according to Figure 4(a) of G04. Nevertheless, the cloud base is located at the correct level (pressure below 900 hPa). Half an hour later, the convective cloud starts to builds up until the 350 hPa level is reached after 5 hours of simulation. This characteristic time is well reproduced by the convective scheme compared to the CRM simulation but the cloud top appears to be lower by 100 hPa. This proper behaviour is a consequence of PCMT continuous formulation of both cloud profile (starting from dry thermals in this particular case) and closure condition (the convective characteristic time ranging from 0.3 h to 1.5 h from shallow to deep convection). For the SEt experiment, the cloud build-up is quite instantaneous at 1030 h, the maximum extension being reached at 1300 h, i.e. about 3 h before than what is produced by REF or the CRM. A large amount of moisture is detrained in the upper levels (above 400 hPa) giving rise to an anvil with a 100% cloudiness. This behaviour of the SEt experiment is clearly typical of the response to a weaker entrainment rate, as seen in the previous sub-section. It is worth noting that this fast growing convection was also found in the majority of SCM taken into account in G04 (see Figure 13(b) of G04), being an indication of the rather weak entrainment rates used in these convection schemes at this time.

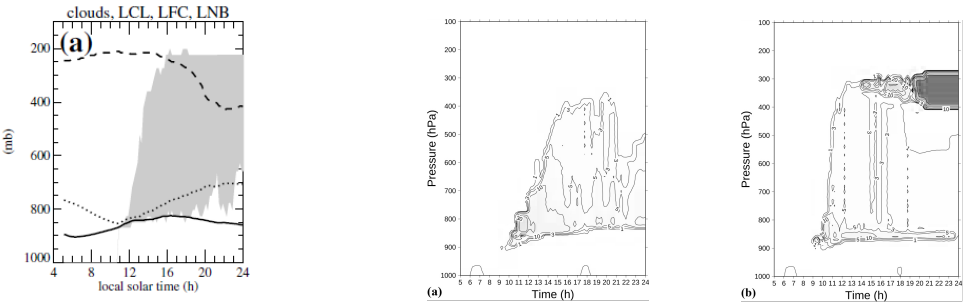

CRM for information (Figure 4(a) of G04). **Figure 3.** Time evolution of the SCM cloud fraction (%) for (a) REF and (b) SEt.

2.2.2 Diurnal cycle of marine stratocumulus

The single column case study selected for this sub-section has been designed by Duynkerke *et al.* (2004), hereafter called Du04. This is a marine stratocumulus case study set-up with the help of observations from the First ISCCP Regional Experiment (FIRE) field campaign in July 1987. Further to the observations, results from 6 LES are reported in Du04; these results together with the observations will be used to evaluate the present SCM simulation. The initial state is characterised by a significant jump of 12 K in potential temperature and -3 g kg^{-1} in specific humidity at cloud top (600 m) (see Figure 2 of Du04). The main forcings consist of a large-scale subsidence rate being balanced above the boundary layer by large-scale horizontal advection terms of temperature and

humidity. The radiation scheme is fully interactive allowing the development of a diurnal cycle. The surface flux scheme is also interactive (as for the BOMEX case study).

Figures 4(a)-(d) show the time evolution of the simulated cloud fraction over a 48 h period, for REF, SEt, REF without convection and REF without entrainment at the top of the boundary layer respectively. The observations and LES results show a 100% cloud fraction during the 2-day period (see Figure 5 of Du04), characterised by a diurnal cycle with a minimum cloud depth in the afternoon (due to the short wave radiation heating), the mean cloud top (base) being located at 600 m (200 m respectively). REF experiment exhibits some diurnal phase locking during the second day of simulation (after a first day spin-up), with a lowering of the cloud top starting at around 0800 h (local time) and ending after 2000 h; the cloud top appears to be lower by around 100 m compared to observations and LES, the present vertical resolution providing only 10 levels below 700 m. SEt experiment presents a very similar cloud evolution, with a slightly larger variability due to more active convection induced by the weaker entrainment rate. Nevertheless, the convection scheme is not the predominant one for this case study. This is the turbulent scheme the most important in order to properly simulate the stratocumulus time evolution, as shown in Figure 4(c). The added value of the convection scheme is to realistically delay (advance respectively) the cloud top descent (ascent respectively) by around two hours, thanks to the increased non local mixing. By far, the planetary boundary layer entrainment is the main parametrised process allowing a sufficient mixing to sustain a correct stratocumulus elevation, as seen on Figure 4(d). This parametrised process has been introduced in the turbulence scheme by Guérémy (2005) following Grenier and Bretherton (2001), computing an increased exchange coefficient at the top of the planetary boundary layer.

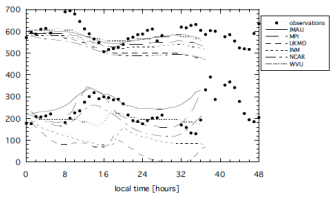

CRM for information (Figure 5 of Du04).

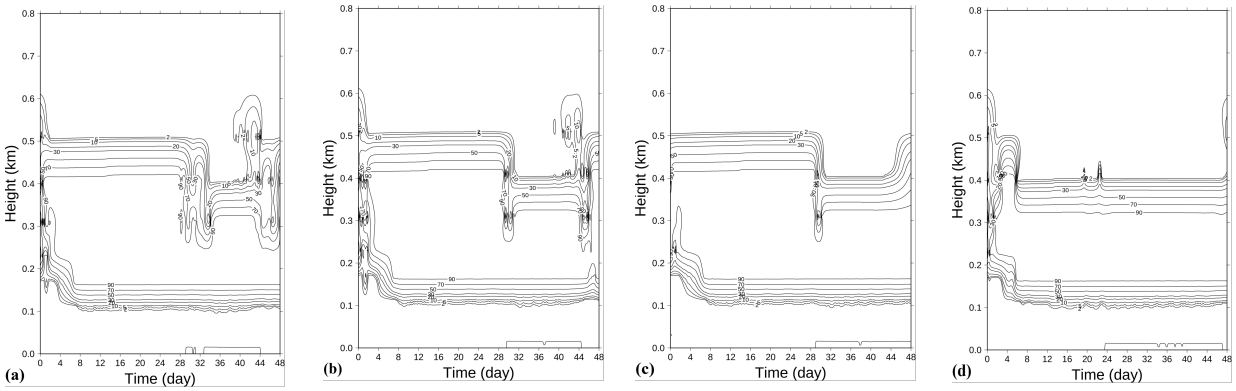

Figure 4. Time evolution of the SCM cloud fraction (%) for (a) REF, (b) SEt, (c) REF without convection and (d) REF without entrainment at the top of the boundary layer.

Figure 5 shows the time evolution of the modelled liquid water path (LWP) for the REF experiment. As for the cloudiness evolution, LWP is characterised by a rather correct diurnal cycle during the second day of simulation, depicting a local minimum around 1800 h (see Figure 4 of Du04); nevertheless, the average value of LWP is smaller than that of observations and LES, being consistent with a smaller cloud depth (see above).

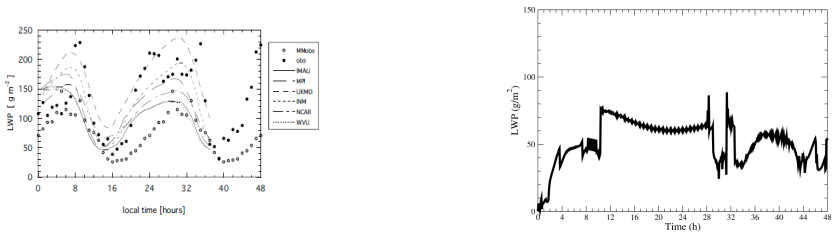

CRM for information (Figure 4 of Du04). **Figure 5.** Time evolution of the SCM liquid water path for REF.

3. GCM evaluation

Beyond the SCM evaluation discussed in the previous section, the performance of the new convection scheme is assessed in GCM mode. The model used in the previous section (ARPEGE-Climat) is now considered in a three-dimensional global geometry. Ten year coupled simulations have been carried out, using that model (with a linear triangular truncation of 159 waves and 91 vertical levels, i.e. Tl159l91, corresponding to a 125 km grid mesh) together with the ocean model NEMO (Madec, 2008) at a 1° horizontal resolution and 42 vertical levels. The period considered in terms of initial conditions and external forcings is the 1980 decade. Three experiments are analysed following the sensitivity study performed in the previous section: REF, SEt and SEp. The GCM evaluation is discussed in three sub-sections: the first one is devoted to mean climate, the second one to intraseasonal variability and the last one to interannual variability.

3.1 Mean climate

Figure 6 shows the zonally averaged temperature bias versus ERA-Interim climatology (Dee *et al.* 2011) for the REF experiment, in winter (DJF) and summer (JJA). There is an overall negative bias of the order of 1 K, except in low levels where the bias is close to zero and around the tropopause where the negative bias reaches 4 K. The use of a new version of NEMO with 75 vertical levels (providing a larger vertical resolution in the ocean mixed layer) decreases the bias in the mid-latitude summer hemispheres (not shown). Moreover, with a higher atmospheric horizontal resolution of about 50 km grid mesh, the biases are reduced everywhere by about 0.3 K and the tropopause negative bias is reduced to 3 K, (not shown).

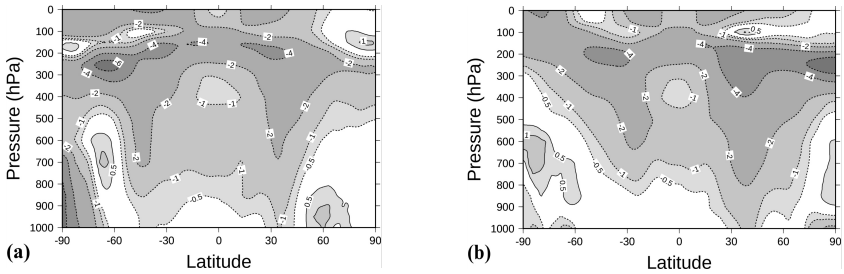

Figure 6. Zonally averaged temperature bias (GCM minus ERA-Interim climatology, in K), (a) DJF and (b) JJA.

Taking into account the results of sub-section 2.2 on the scheme sensitivity, zonally averaged specific humidity biases (versus ERA-Interim climatology) for the REF, SEt, SEp experiments are depicted in Figures 7(a)-(c) respectively, in winter (DJF) and summer (JJA). The REF bias appears to be quite reasonable, except in the northern hemisphere in JJA with significant negative values. As for the temperature bias (see previous paragraph), the use of a new version of NEMO with 75 vertical levels allows a drastic reduction of that negative bias (not shown). The main result here is the same response of the sensitivity experiments SEt and SEp as the one discussed in sub-section 2.2: i.e., specific humidity increase for SEt and specific humidity decrease for SEp. This relative behaviour clearly appears in Figures 7(a)-(c) all over the globe, SEt magnitude of the response being larger than that of SEp.

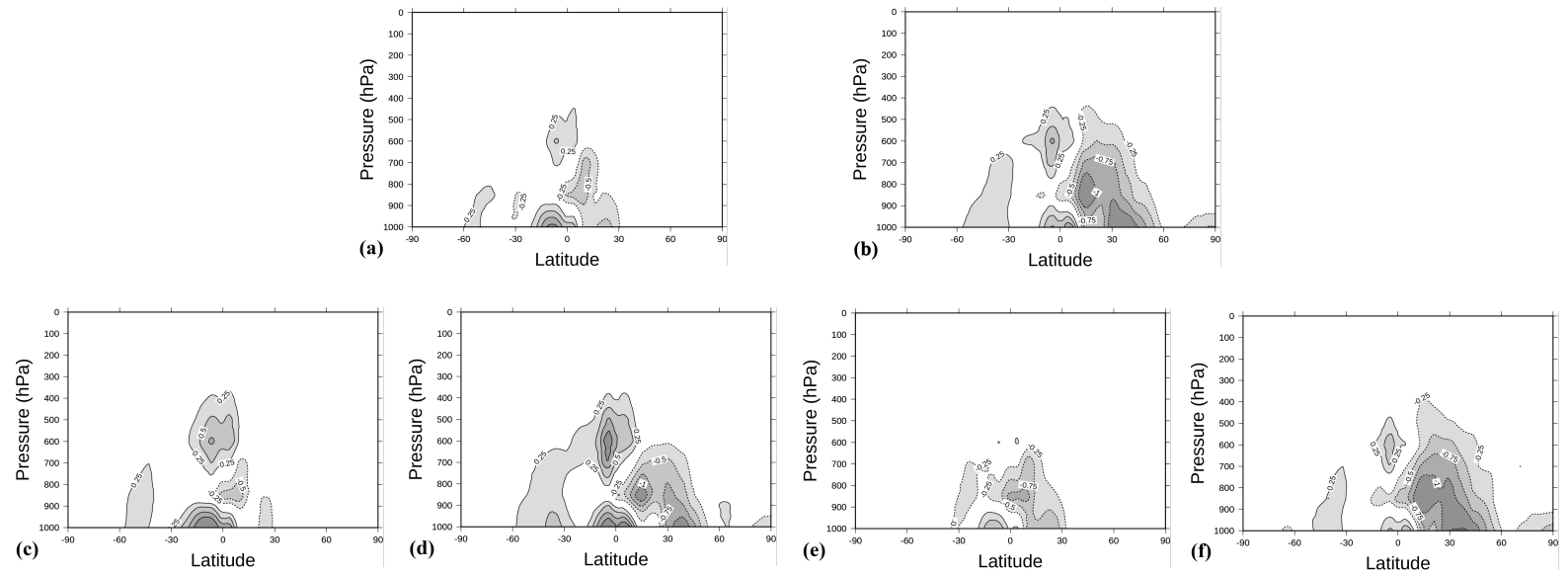

Figure 7. Zonally averaged specific humidity bias (GCM minus ERA-Interim climatology, in g kg^{-1}) for (a) REF DJF (b) REF JJA, (c) SEt DJF (d) SEt JJA and (e) SEp DJF (f) SEp JJA.

Nevertheless, the coupled GCM response is more complex than the SCM one due to all the feedbacks in place in the former. Table 1 presents a series of globally averaged energy fluxes (in W m^{-2}) and the 2 m temperature (in °C) for the three experiments together with the corresponding value from observations or analysis. Considering the surface downward long-wave radiation flux

(Surf_d_LWR), it appears that the REF experiment exhibits a value in line with observations. These observations taken from Wild *et al.* (2013) are valid for the 2000 decade; REF value corresponding to the 1980 decade is indeed slightly smaller. Consistently with the excess (deficit respectively) of specific humidity in SEt (SEp respectively), Surf_d_LWR is larger (smaller respectively) for SEt (SEp respectively). It is worth noting that the difference with REF is greater with SEt versus SEp, as already mentioned concerning the humidity response. Contrary to SCM simulations, coupled GCM simulations are impacted by many feedbacks. The surface energy budget and the surface temperature are modified by these feedbacks, as shown in Table 1. The two sensitivity experiments are affected by a positive feedback, which tends to further increase the excess of humidity in SEt (the deficit of humidity in SEp respectively). REF surface energy budget and 2 m temperature are comparable to the observations. But, SEt is characterised by a larger surface energy budget and consequently by a larger 2 m temperature, while being smaller in SEp. The SEt surface energy budget increase is mainly due to a larger net surface radiation flux induced by a smaller amount of low clouds (main increase of humidity at higher levels); surface turbulent fluxes are decreasing at the same time by a lesser extent, because of smaller surface humidity gradients. In SEp experiment, the main reason causing the surface energy budget decrease is the consequence of larger surface turbulent fluxes (induced especially by an increase of surface humidity gradients), despite the larger net surface radiation flux (as in SEt) induced by a smaller amount of medium clouds. Finally, the top net radiation fluxes are close to the observed one, taking into account the two different periods concerned. The decrease of the cloud amount in both sensitivity experiments (especially SEp) provides the main explanation of the top net short-wave radiation flux increase (versus REF). SEp top net long-wave radiation flux is larger than that of REF due to much weaker convective induced high cloud amount.

Energy fluxes (W m^{-2}) and T2m	Wild *et al.* (2013) or ERA-I	REF	SEt	SEp
Surf_d_LWR	342 *(338, 348)*	341.0	343.6	339.4
Surf_energy_bud	0.6 *(0.2, 1.0)*	0.9	1.6	0.6
T2m (°C)	14.1 *(ERA-I)*	14.0	14.4	13.7
Top_net_SWR	240 *(240, 245)*	238.4	239.1	239.6
Top_net LWR	239 *(236, 242)*	237.6	237.5	239.1

Table 1. Globally averaged energy fluxes and 2 m temperature of observations and the 3 experiments REF, SEt and SEp.

Figures 8(a)-(b) illustrate the comparison of winter (DJF) Global Precipitation Climatology Project (GPCP) rain amount (Huffman *et al.*, 2001) versus that of REF experiment. There is a close resemblance between the two fields. One of the main discrepancy consists of the so-called “double ITCZ” pattern, with a south Pacific convergence zone being too zonal around 150°W. This feature is emerging in coupled mode only (not shown) and might be partly due to insufficiencies in the

present ocean model at a 1° horizontal resolution; the use of an increased vertical resolution (see previously) does not improve the simulation in that matter (not shown). The climatological precipitation pattern of both sensitivity experiments is very similar to the one of REF. SEt as SEp produce less precipitation in the core of the ITCZ, but slightly more around (not shown), which tends to broaden the ITCZ. In the extra-Tropics, SEt is slightly more rainy than REF in regions of shallow convection (as expected), while SEp does not show any clear signal. Globally averaged, the rain amount of REF reaches 3.04 mm day^{-1}, being equal to the one of SEt; the globally averaged rain amount of SEp is larger than the one of REF, but only by 1%.

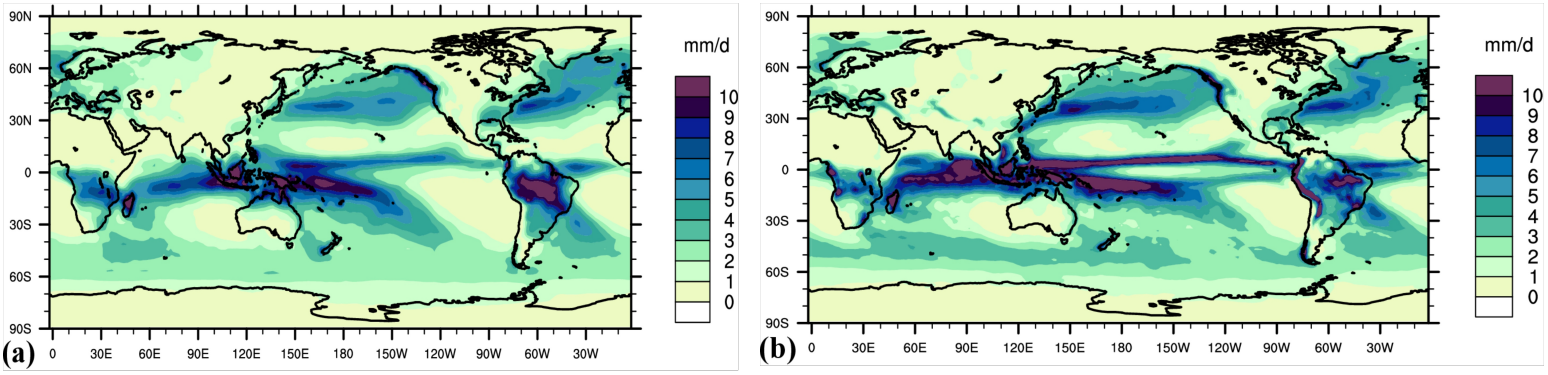

Figure 8. Precipitation climatology in DJF (in mm day^{-1}) for (a) GPCP and (b) REF.

3.2 Intraseasonal variability

Further to the evaluation of the mean climate, the performance of the model including PCMT will be assessed in terms of variability at subseasonal scales. First, results concerning the diurnal cycle will be shown considering both REF and SEt experiments. Second, the distribution pattern of daily precipitation will be discussed, including the results of both sensitivity experiments. Third, an evaluation of the space-time variability of outgoing long-wave radiation (OLR) in the tropics (as a proxy for convectively driven waves) will be presented, here also including the results of both sensitivity experiments.

3.2.1 Diurnal cycle

Diurnal cycle is a challenging process to simulate using large-scale models including convection schemes. However, some recent studies have reported significant improvements in that respect (Takayabu and Kimoto 2008; Bechtold *et al.* 2014). In subsection 2.2.1, a rather realistic diurnal cycle simulation of a one-dimensional continental case study has been shown. It has been stressed that the proper behaviour of the SCM simulation was the consequence of PCMT continuous formulation of both cloud profile and closure condition (expressed in terms of buoyancy). Beyond the SCM simulation, it appeared noteworthy to show the ability of the GCM simulation, in which everything is interacting together, to represent this specific variability. The precipitation variable has been chosen for that purpose, in so far as it is driven by the prognostic microphysics, being a novel aspect of PCMT, which should provide an a priori better diurnal variability in further delaying that

process beyond all other aspects of the scheme. Figure 9 displays the phase of the diurnal cycle maximum, expressed in local solar time, for the TRMM dataset (Huffman *et al.*, 2007) over a two year period (2016-2017) and for the two first years of both REF and SEt GCM simulations. To produce these figures, 3-hourly precipitation rates have been cumulated over two years, for the eight times of the day (731 3-hourly fields). Phase of the diurnal harmonic is then calculated using Fourier analysis.

The TRMM radar observations clearly shows the well known different phase over continent and ocean. It is located in the late afternoon, up to the first part of the night in the center of some continental regions, for the former and in the late night to early morning for the latter. Interesting spatial variations of the phase appear at the interface of ocean and continent in some regions. Starting from the coast to the open sea, a phase shift from the late night to the afternoon shows up in the Maritime Continent and off the Central American and West African coasts for example, as an indicator of the deepening of convection away from the coast. On the other hand, starting from the coast to the inner continent, a phase shift from afternoon (or even noon) to late night appear over North-Eastern Amazonia and over the Maritime Islands for example, here also being an indicator of the delayed convection off the coast. The phase of the REF diurnal cycle presents the same spatial pattern as the one of TRMM, but being in advance of roughly two hours. This constitutes a rather good result, comparable to that obtained by Bechtold *et al.* (2014) for instance. The previously discussed spatial variations of the phase over particular interface regions are also reproduced by the REF simulation. Concerning the phase pattern issued from SEt experiment, there is a very close resemblance to that of REF. However, SEt phase is also two hours in advance compared to REF phase, almost everywhere over the globe. It is worth to notice that this phase lag is similar the one discussed in subsection 2.2.1, devoted to the one-dimensional continental diurnal cycle case study.

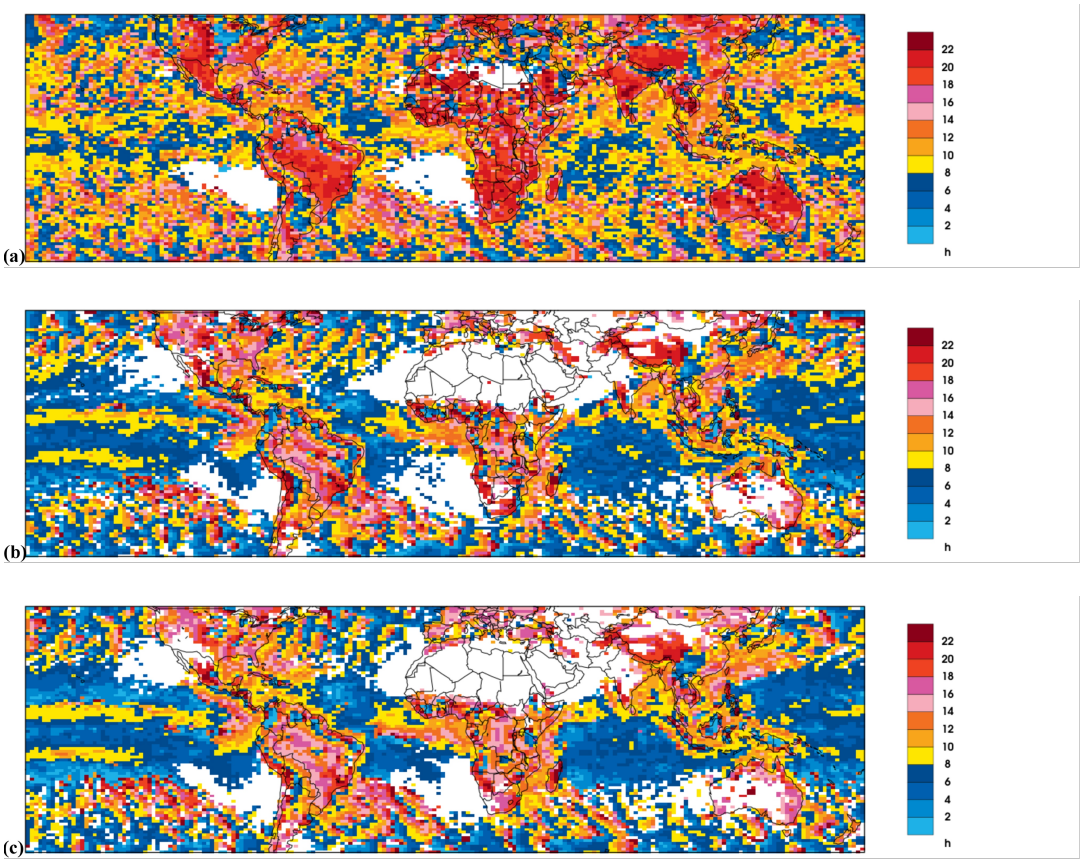

Figure 9. Diurnal phase (local solar time) of precipitation for (a) TRMM, (b) REF and (c) SEt over a two year period.

Figure 10 shows the diurnal cycle from TRMM (2016-2017) together with REF and SEt GCM simulations (two first years) over two particular continental regions, Amazon (70°W-40°W, 20°S-0°) and West Africa (15°W-15°E, 5°N-15°N). REF diurnal cycle appears to be almost in phase with TRMM. More precisely, REF precipitations are starting about 1h30 in advance compared to TRMM, but REF maximum is located at the right time. Interestingly, the precipitation maximum occurs earlier in Amazon versus West Africa, due to the moister environment of the former region. Furthermore, the Amazonian maximum rain amount is larger than the West African by 40%. The REF maximum rain amount negative bias is larger in Amazon, where convection is less aggregated, than in West Africa, 55% versus 30%; this rain amount discrepancy decreases with larger resolution (from 125 km to 50km, for example; not shown). The 2-hour advance of the rainfall maximum from SEt compared to REF, already mentioned above at global scale, is clearly seen in Figure 10, for the two considered regions. It is worth noting that REF rain amount is larger (smaller respectively) than SEt rain amount over West Africa (Amazon respectively). This difference might be explained by the fact that convective rain is strongly linked to African Easterly Waves in a positive feedback process; with a larger entrainment, the convective precipitation tends to be more intense with a smaller space scale, which tends in return to intensify the relatively small scale AEW. This constitutes a salient result of the present paper, which will be further argued in the following subsections.

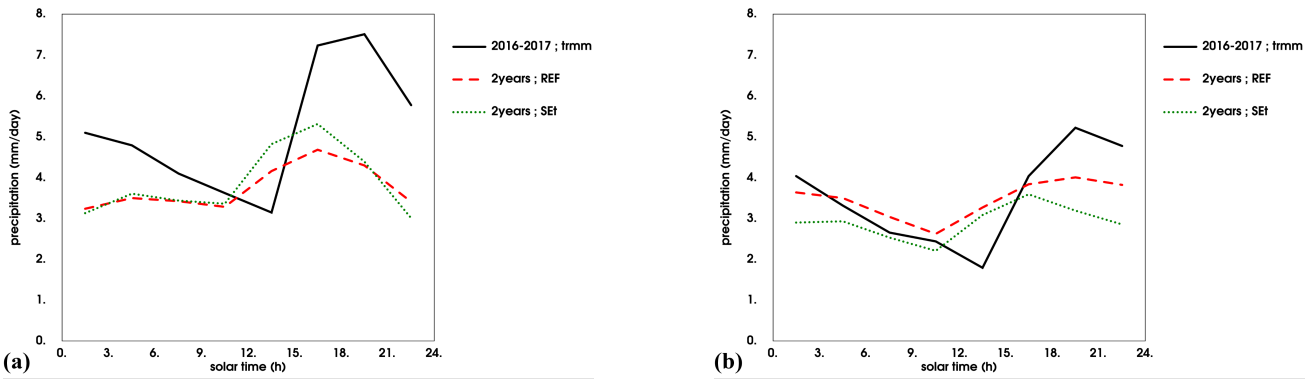

Figure 10. Diurnal cycle of precipitation from TRMM, REF and SEt over (a) Amazon (70°W-40°W, 20°S-0°) and (b) West Africa (15°W-15°E, 5°N-15°N).

3.2.2 Distribution of daily precipitation

For the sake of simplicity, and because the focus of the paper is put on convection, only the tropical precipitation (from 30°S to 30°N) is considered in this section. The distributions of daily precipitation are computed for the two extreme seasons (DJF and JJA) over the 10 year period of the coupled simulations over land and over sea. As there are more land points in the summer season in the northern hemisphere, Figure 11 shows the distributions of daily precipitation for DJF over sea, and for JJA over land. The distributions are computed with regular bins of 1 mm/day, using a frequency log axis as ordinate. Two different reference datasets are plotted: GPCP (Huffman *et al.*,

2001) and Tropical Rainfall Measuring Mission (TRMM) (Huffman *et al.*, 2007). Both datasets are derived from satellite observations and rain gauges. TRMM also includes radar observations. The GPCP daily precipitation dataset is available at a resolution of 1° x 1°, while TRMM native resolution is 0.25° x 0.25°. Here, they are both interpolated at the resolution of the model (around 125 km). Their differences give an idea of the range of uncertainties. However, for extreme precipitations, TRMM might be more trustworthy as it is initially computed at a higher resolution and includes radar observations. REF simulation produces a rather realistic precipitation distribution, both over sea and land. Nevertheless, extreme precipitations are underestimated over sea, compared to TRMM. This was an expected result considering the coarse atmospheric grid used in these simulations compared to that of TRMM. Over land, extreme precipitations are slightly overestimated, taking the previous comment into account; this might be the consequence of a simulated soil being a little too dry in this version of the soil scheme (which has been improved since). SEt precipitation distribution appears to be shifted from that of REF, with more moderate precipitation and less extreme precipitation. This was somehow an expected result, in so far as by lowering the entrainment, the moderate convection is favoured at the expense of extreme convection; in others words, the CAPE consumption by convection is shifted toward moderate events. Finally, SEp precipitation distribution is very similar to that of REF.

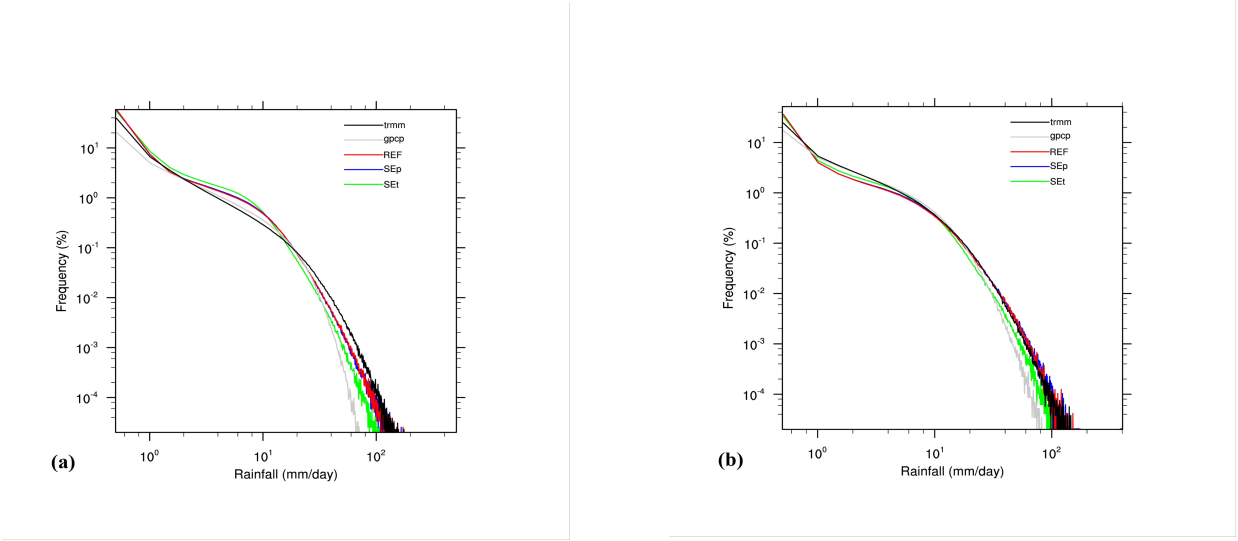

Figure 11. Distribution of tropical daily precipitation (in mm day^{-1}) of (a) DJF over sea and (b) JJA over land. The Y-axis (frequency of occurrence, in %) is logarithmic.

In order to highlight the differences between the 3 experiments, the previous precipitation distributions computed with only 5 bins are shown in Figure 12. These 5 bins correspond to typical regimes of precipitation: i.e., no precipitation, light rain, moderate, heavy and extreme rainfalls. For both DJF over sea in Figure 12(a) and JJA over land in Figure 12(b), two histograms are depicted: with a logarithmic frequency of occurrence on the right hand side highlighting extreme events, and with a linear frequency of occurrence on the left hand side highlighting the dry day events. Concerning REF, further to the already mentioned underestimation of extreme in DJF over sea and slight overestimation of extreme in JJA over land, it appears an underestimation of dry days and an

overestimation of light rain days in DJF over sea. This might be partly the result of the reference uncertainty concerning light rains over sea. The trade wind cumulus regime, representing a major part of light rains over sea, is providing a rain amount of 0.2 mm day^{-1} (Holland and Rasmusson, 1973), which corresponds to the SCM simulated rain amount from the BOMEX case study (see Part I). The shift of SEt distribution compared to that of REF is more clearly seen in Figure 12. With the inclusion of the dry bin, it corresponds to a tightening of the distribution versus REF: there are less dry days and heavy to extreme events, but more light and moderate events. The tightened shape of the distribution obtained with a smaller entrainment rate is definitively more distant from the distribution shape of GPCP or TRMM than that of REF. This constitutes the main result out of the comparison of the precipitation distributions coming from the 3 experiments. SEp distribution shows a slight larger frequency of moderate rain events in both seasons, the frequencies of the other bins being very similar with no systematic differences. This larger frequency of moderate rain events in SEp explains part of the 1% additional rain amount at global scale versus REF (see previous section).

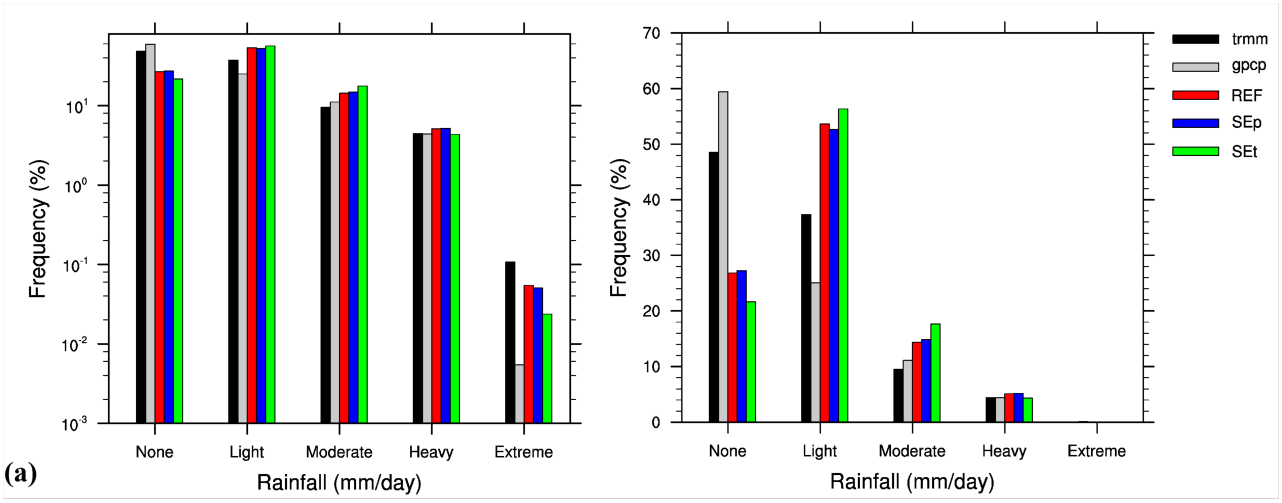

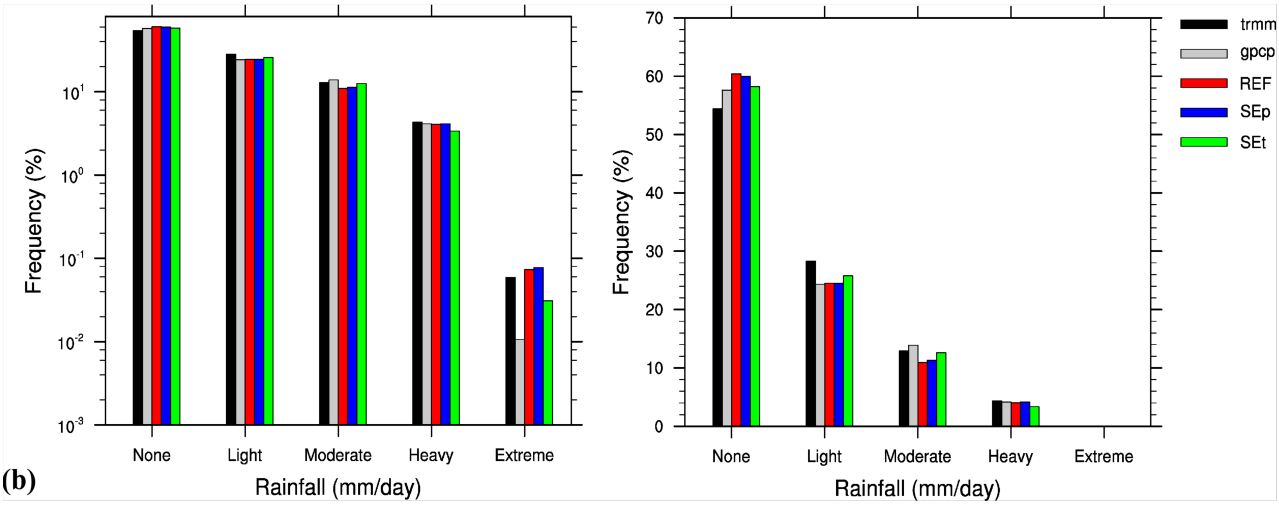

Figure 12. Distribution of tropical daily precipitation (Pr) (in mm day^{-1}) in 5 classes : None : 0 < Pr < 0.01 ; Light ; 0.01 < Pr < 1 ; Moderate : 1 < Pr < 5 ; Heavy : 5 < Pr < 20 ; Extreme : Pr > 20 mm day^{-1}; (a) DJF over sea and (b) JJA over land. The Y-axis (frequency of occurrence, in %) is logarithmic on the right hand side plots, and linear on the left hand side plots.

3.2.3 OLR intraseasonal variability

In the tropics, a significant part of the climate variability is due to equatorial waves (Matsuno, 1966). These waves are strongly associated to convection, and possibly affect the extra-tropics through westward moving Rossby waves (Gill, 1980). Therefore, they constitute a key climate element to be evaluated during the introduction of a new convection scheme, as PCMT. As already reported (Wheeler and Kiladis, 1999; Bechtold *et al.*, 2008), the equatorial wave activity has been evaluated using OLR wavenumber-frequency spectra. The boreal winter season (DJFM) is considered for the sake of simplicity. One hundred twenty daily OLR values, for a 9 year period (1979-1987), over a latitude band 15°S-15°N are used for both satellite observation (Liebmann and Smith, 1996) and GCM simulations. The wavenumber-frequency spectra are computed for each year and averaged over the entire period using a methodology described in Ceron and Guérémy (1999), which provides spectral densities for both zonal and meridional wavenumbers. In this study, the meridional wavenumber spectral densities are summed in order to consider only the zonal wavenumbers. Following Wheeler and Kiladis (1999), a background spectrum is calculated by successive passes of a 1-2-1 filter in frequency and wavenumber. The raw spectrum of the symmetric component is divided by this background to obtain an estimate of the signal standing above the 'red' noise, in a relative way. Figures 13(a)-(d) compare these wavenumber-frequency spectra of the observation (hereafter called OBS) to the GCM simulations (REF, Set and Sep experiments). As in Wheeler and Kiladis (1999), the Kelvin and Rossby dispersion curves are superimposed upon the spectra, using 3 typical tropospheric equivalent depths (12, 25, 50 m). The variance densities are plotted in Figure 13 for relative values larger than 1.1. For the symmetric component, the square root of the OBS total variance is equal to 22 W m^{-2}, being moderately larger in REF and SEt by 25% and slightly larger in SEp by 5%. Thus, these relative spectra could also be compared in terms of absolute values of variance density. Consistently with Wheeler and Kiladis (1999), the OBS spectrum shows three main areas of significant signal: two eastward moving oscillations on the right side, the Madden and Julian oscillation (MJO) for wavenumbers from 1 to 4 and frequencies from 2 to 4 (30 to 60 days) and Kelvin waves along their dispersion curves, and one westward moving oscillation on the left side, corresponding to Rossby waves here again along their dispersion curves. REF simulation spectrum shows a rather good agreement with the OBS one. The main discrepancy appears in the MJO signal. The REF MJO signal is weaker than the OBS signal, with a tendency to show a larger spread in space and time (i.e., from 40 to 60 days for the latter compared to a rather sharp peak at 60 days in the former). The previous version of the physics implemented in ARPEGE-Climat and operated in CNRM-CM5 produces more variance in the MJO area, but less variance in the eastward moving Kelvin wave area at smaller scales (see Figure 4(f) of Hung *et al.*, 2013). Moreover, with the present convection scheme, REF coupled simulation is providing a space-time spectrum among the best ones from CMIP5 GCM as reported in Hung *et al.* (2013). SEt experiment shows a shift toward larger scales both in space and time for periods greater

than 12 days. At the same time, there is less variance for periods shorter the 12 days, together with smaller phase speeds in the eastward moving Kelvin wave area. Interestingly, this tendency for smaller phase speed and larger scale of synoptic waves has also been found in a recent study devoted to the simulation of African easterly waves using PCMT with a lower value of the entrainment rate (Leger, supervised by Guérémy *et al.*, 2015). In this study, the reduction of convective entrainment induced a larger scale of aggregated convection (consequence of both easier triggering and moister environment) giving rise to larger scale associated easterly waves. On the other hand, SEp shows less (more respectively) variance at large (small respectively) scale. The insufficient tropospheric moisture to sustain long-live meso-scale convective systems (MCS) might be a good candidate to explain such a behaviour. This is a key result of the sensitivity study discussed along the present paper from SCM to GCM experiments: a decrease of entrainment (increase of auto-conversion respectively) induces a larger (smaller respectively) tropospheric humidity amount which in turn, as a positive feedback, tends to increase (decrease respectively) the scale of MCS and associated convectively driven waves.

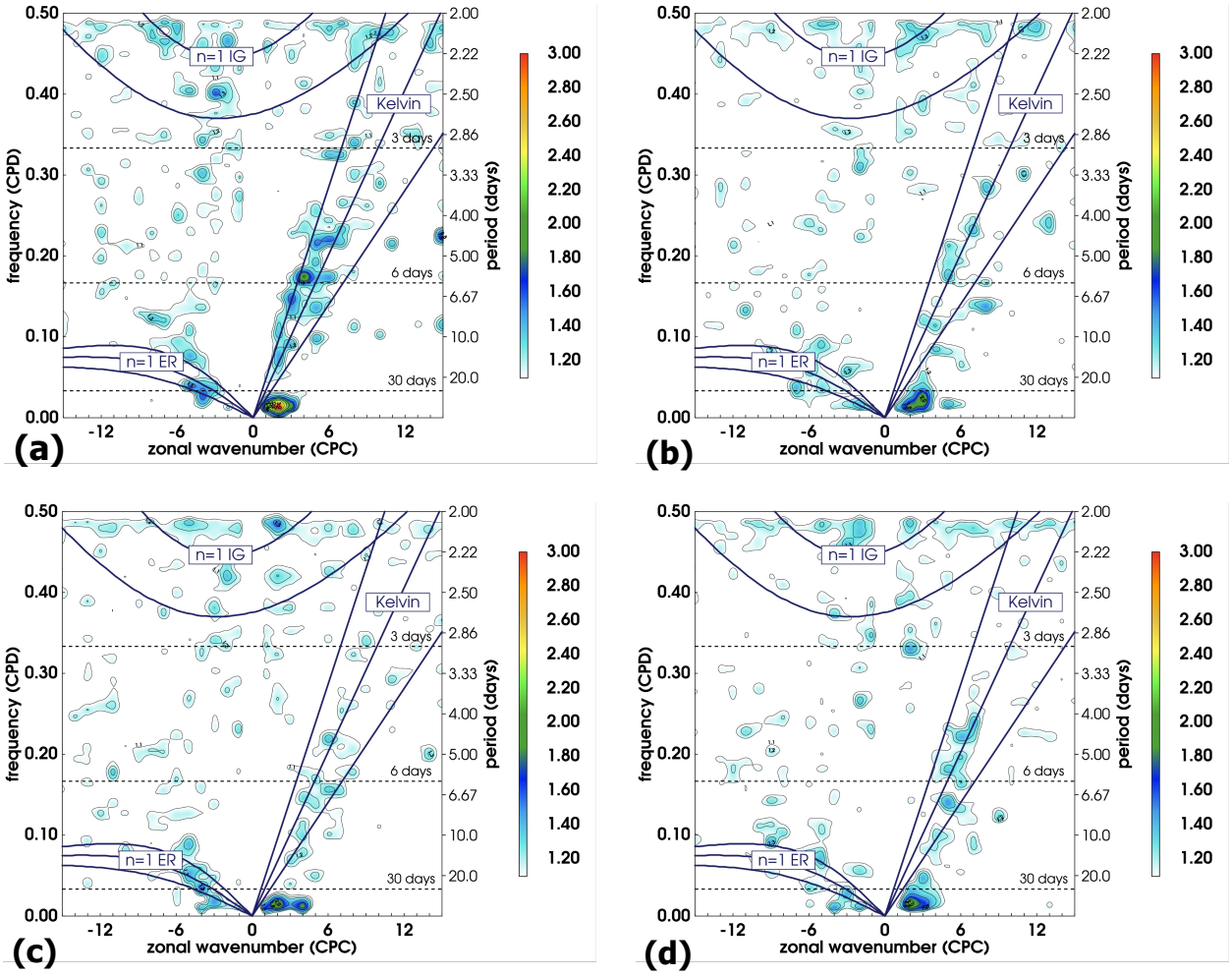

Figure 13. Normalized space-time spectra (15° S to 15° N, December to March -120 days- over 10 years), of (a) satellite-observed OLR, (b) REF, (c) SEt and (d) SEp simulated OLR; eastward propagating left, westward right. Dispersion curves of Kelvin (left) and Rossby (right) waves for equivalent depths of 12, 25, 50 m (from bottom to top).

In order to investigate the MJO activity in more details, its variance from observed and simulated OLR is depicted in Figure 14. The MJO signal was extracted as in Wheeler and Kiladis (1999), considering wavenumbers from 1 to 4 and frequencies from 2 to 4 (30 to 60 days) for eastward propagating waves only. Further to the possibility of selecting one particular direction of propagation, the methodology described in Ceron and Guérémy (1999) allows to obtain a partition between stationary and propagating phenomenons on any longitude-latitude domain. In order to put the emphasis on the propagating part of MJO, the variance shown in Figure 14 encompasses only the contribution coming from eastward propagating waves. The observed OLR variance pattern extends from the eastern Indian Ocean to the western Pacific Ocean along 10°S, with a maximum located north of Australia. The REF simulated OLR variance pattern is well located but too much elongated in the zonal direction on the equatorial Indian Ocean. The variance magnitude is weaker by around 50% (or even more in the north of Australia) than the observed one; this constitutes a rather good result compared to that of CMIP5 models (see Figure 7(a) of Hung *et al.* (2013)). Consistently with what has been found for the space-time spectrum (Figure 13(c)), SEt shows a larger scale variance pattern (mainly wave number 1 and 2) than that of REF, without local maximum in the north of Australia. SEp presents less variance than REF, with a smaller scale pattern (wave number 4), here also consistently with the information shown in the space-time spectrum (Figure 13(d)). The maximum of variance is located south of Indonesia, in the west of the observed and REF ones.

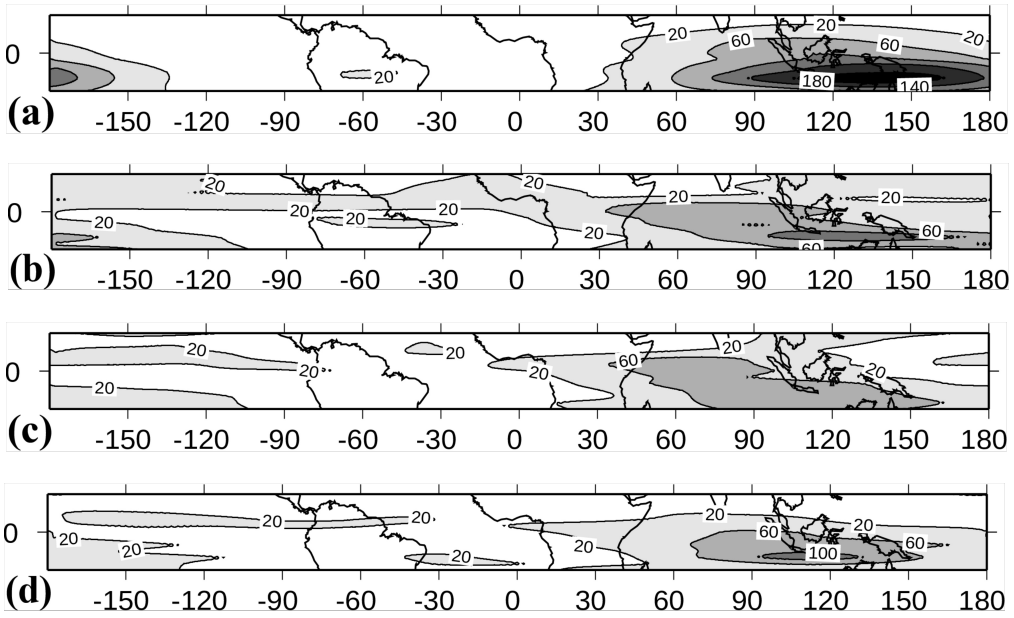

Figure 14. Variance of (a) observed OLR, (b) REF, (c) SEt and (d) SEp simulated OLR (in W^2/m^{-4}) on the MJO space-time domain.

3.3 Interannual variability

El Niño-Southern Oscillation (ENSO) is a major mode of the interannual variability of the coupled ocean-atmosphere system in the tropics. Furthermore, ENSO generates robust climatological

impacts in the extra-tropics, due to induced mid-latitude Rossby waves in the troposphere (Gill, 1980). This is the reason why the focus has been made on this particular mode of variability to get a first insight on the model skill and on its sensitivity to convective entrainment (SEt experiment) and precipitation efficiency (SEp experiment).

The regression of the global geopotential height at 500 hPa (hereafter called Z500) onto the first principal component of the tropical Pacific SST provides an interesting and synthetic diagnostic of the atmospheric response to ENSO. Figure 21 shows such a diagnostic for ERA-Interim reanalysis and REF, SEt and SEp simulations, for the boreal winter season. The 10 year period of the coupled simulations (1979-1988) has been used to perform an SST EOF analysis on a tropical Pacific domain (30°S-30°N, 160°E-60°W) during DJF of each of the four previously mentioned datasets. The 10 year DJF covariances between the first principal component of the tropical Pacific SST and Z500 are computed at each grid point over the globe to get the corresponding regressed values of Z500 (expressed in terms of anomalies in meters). Over the northern Pacific Ocean, a very clear Pacific/North American pattern (PNA) appears on the ERA-Interim plot (Figure 15(a)), with the alternation of four positive and negative extrema starting east of Hawaii and ending in the south-east of the USA. Moreover, a West Pacific pattern (Barston and Livezey, 1987) shows up with a typical positive-negative dipole on the western part of the basin. Other anomalies are also seen all around the globe, but for the sake of concision, they are not discussed in this paper. Over the northern Pacific Ocean, REF simulation (Figure 15(b)) presents a rather similar pattern compared to that of ERA-Interim, the magnitude of the response to ENSO being slightly larger. The tropical convective response produced by SEt experiment has a larger scale (and a smaller magnitude) compared to that of REF (Figure 15(c)). Interestingly, the relative behaviour of SEt versus REF in terms of the scale of the response is comparable for both intraseasonal and interannual variability. Consequently, the response of Z500 to ENSO is altered in the northern extra-tropical Pacific basin (and elsewhere). On the other hand, the tropical convective response produced by SEp experiment has a smaller scale (and a smaller magnitude) compared to that of REF (Figure 15(d)). Here also, the relative behaviour of SEp versus REF in terms of the scale of the response is comparable for both intraseasonal and interannual variability; in the same manner as for SEt, the response of Z500 to ENSO is altered in the northern extra-tropical Pacific basin (and elsewhere).

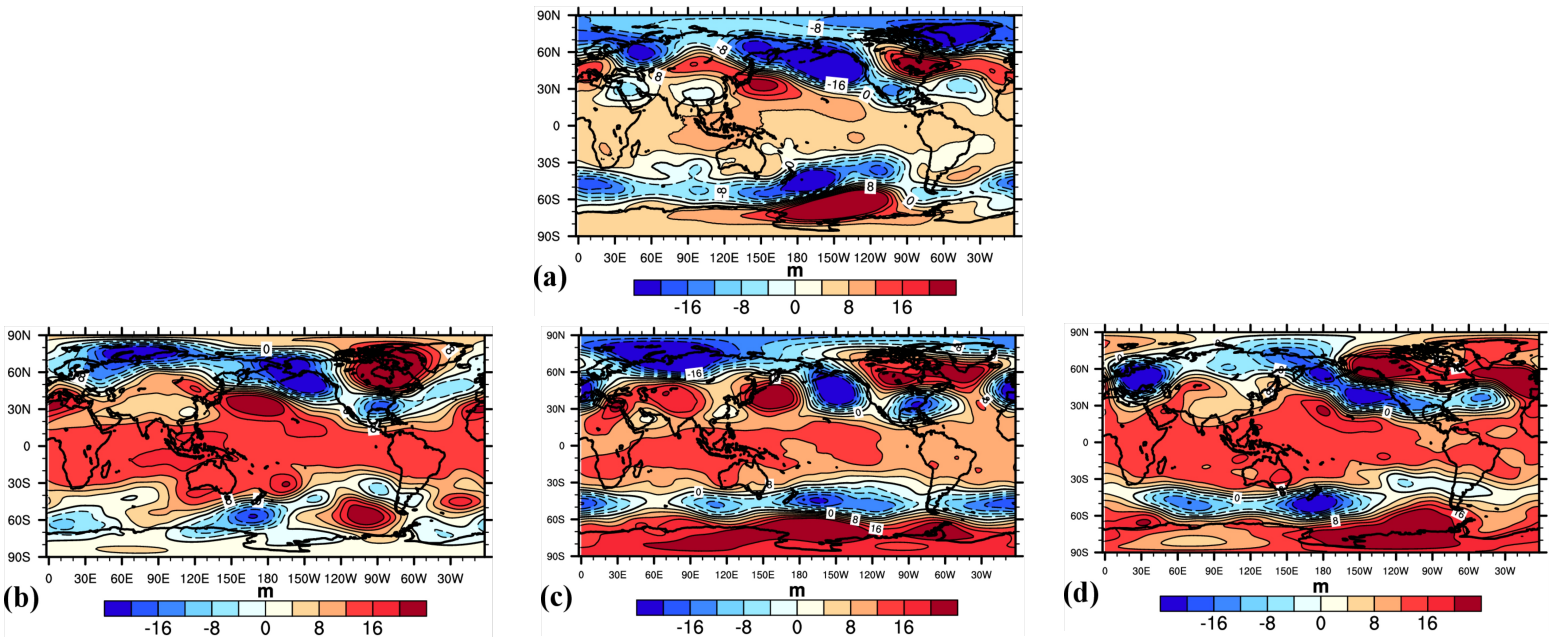

Figure 15. Z500 regression onto the first principal of the equatorial Pacific SST of (a) ERA-Interim, (b) REF, (c) SEt and (d) SEp (in m).

4. Conclusions

A new convection scheme (PCMT) evaluation and sensitivity has been described.

As a necessary first step of this work, several SCM simulations have been analyzed. In order to design sensitivity experiments to be performed all along the present article, two scheme parameters have been selected, the turbulent entrainment rate and the solid auto-conversion rate: more specifically, decreasing the maximum turbulent entrainment rate by 56% (i.e. $4 \times 10^{-5} Pa^{-1}$) defining SEt a reduced entrainment experiment, and increasing the solid auto-conversion rate by 57% (i.e. $55 \times 10^{-4} s^{-1}$) defining SEp an increased precipitation efficiency experiment, to be compared to REF the reference experiment. Considering the case study proposed by Derbyshire *et al.* (2004) devoted to the sensitivity of moist convection to the environment, SEt exhibits a large difference to REF that manifests itself notably by an exaggerated depth of shallow convection, associated to a moister environment, entering into a positive feedback; SEp shows a smaller difference to REF that consists in a narrower convective depth, associated to a drier environment, entering also in a positive feedback.

Then, a first evaluation of PCMT has been conducted in SCM mode, making use of two additional case studies dealing with diurnal cycle of convection. Thanks to its continuous character (resulting from its continuous formulation of both cloud profile and closure condition), PCMT is able to well represent the continental diurnal cycle of this case study proposed by Guichard *et al.* (2004). Moreover, SEt experiment shows a different behaviour characterised by a too fast growing convective system reaching its maximum extension 3h earlier than what is simulated by REF and the reference CRM. Concerning the diurnal cycle of marine stratocumulus taken from Duynkerke *et al.* (2004), PCMT enables a realistic delay (advance respectively) of the cloud top descent (ascent respectively) by around two hours, thanks to the increased non local mixing added to the predominant local diffusive one (coming from the turbulence scheme).

As a second evaluation stage, the skill of PCMT has been assessed in GCM mode. Ten year coupled simulations have been carried out over the 1980 decade, with a linear triangular truncation of 159 waves (corresponding to a 125 km grid mesh) and 91 vertical levels, together with the ocean model NEMO (Madec, 2008) at a 1° horizontal resolution and 42 vertical levels. Three experiments have been analysed following the sensitivity study performed in SCM mode: REF, SEt and SEp. The zonally averaged temperature bias (versus ERA-Interim) presents an overall negative bias of the order of 1 K, except in low levels where the bias is close to zero and around the tropopause where the negative bias reaches 4 K. Specific humidity field is particularly discriminant for the three experiments. Indeed, the zonally averaged humidity bias (versus ERA-Interim), being reasonable for REF, shows a clear positive (negative in a lesser extent respectively) shift for SEt (SEp respectively) consistently with the SCM responses, which constitutes a salient result of this article. As expected, the GCM response is more complex, with positive feedbacks appearing in both sensitivity experiments due to changes in their surface energy budget. REF precipitation climatology is close to that of GPCP, the main discrepancy being a tendency toward the so-called

“double ITCZ” pattern. SEt and SEp tends to broaden the tropical convergence zones, with less precipitation in the centre and more around.

Beyond the simulated mean climate, some aspects of its variability has been evaluated. Starting with the phase of the precipitation diurnal cycle, REF simulation presents a similar spatial pattern as the one of TRMM, but being in advance of roughly two hours. While also exhibiting a close spatial pattern, SEt simulation shows a phase advance of two hours compared to REF, being consistent with the results discussed using the SCM mode. Considering the diurnal cycle of both Amazonian and West African regions, REF precipitation maximum is in phase with TRMM, but with a 1.5-hour advance in the precipitation start. Secondly, it has been shown that the REF distribution of tropical daily precipitation is very close to that of the references GPCP and TRMM. The main difference consists of an underestimation of dry days and an overestimation of light rain days over sea, which might be partly the result of the reference uncertainty concerning light rains over this particular surface. Interestingly and somehow expected, SEt exhibits a clear tightening of the distribution versus REF, with less dry days and heavy to extreme events, but more light and moderate events; whereas SEp distribution shows only a slight larger frequency of moderate rain events, explaining the 1% additional rain amount at global scale versus REF. Concerning the intraseasonal variability of tropical OLR (used as proxy for convectively driven waves), REF simulation space-time spectrum shows a rather good agreement with the observed one. SEt experiment presents a shift toward larger (smaller respectively) scales both in space and time for periods longer (shorter) than 12 days. On the other hand, SEp shows an opposite behaviour in terms of its main space-time scales of variability. This constitutes a key result of the sensitivity study discussed along the present article from SCM to GCM experiments: a decrease of entrainment (increase of auto-conversion respectively) induces a larger (smaller respectively) tropospheric humidity amount which in turn, as a positive feedback, tends to increase (decrease respectively) the scale of MCS and associated convectively driven waves. The MJO signal has been extracted considering wavenumbers from 1 to 4 and frequencies from 30 to 60 days for eastward propagating waves only, in order to get its corresponding spatial pattern of variance. REF shows a correct location of the MJO variance (extending from the eastern Indian Ocean to the western Pacific Ocean along 10°S), but with a weaker amplitude by around 50%, which is a rather good result compared to CMIP5 models Hung *et al.* (2013). Consistently with what has been found for the space-time spectrum, SEt shows a larger scale variance pattern (mainly wave number 1 and 2) than that of REF, while SEp presents a smaller one (wave number 4). Finally, in order to get a first insight on the model skill in terms of interannual variability, the regression of the global geopotential height at 500 hPa onto the first principal component of the tropical Pacific SST in winter (DJF) has been plotted as a synthetic diagnostic of the atmospheric response to ENSO. Over the northern Pacific Ocean, very clear Pacific/North American and West Pacific patterns appear with ERA-Interim used as a reference. REF simulation presents a similar pattern, the magnitude of the response to ENSO being slightly larger. The tropical convective response produced by SEt (SEp respectively) experiment has a larger (smaller respectively) scale compared to that of REF. Here also, the scale dependency of the sensitivity experiment response is of the same nature. As a consequence of the altered response in the tropics, the mid-latitude geopotential height anomalies are less well represented by both SEt and SEp.

It is worth noting that PCMT convection scheme included in version 6 of ARPEGE-Climat and in the same manner in ARGEGE short to medium range weather forecast is now used in operational seasonal and medium range forecast, and will be used for the forthcoming CMIP6 simulations. Nevertheless, work is still in progress in order to possibly envisage its use for the short range numerical weather forecast. Additional evaluations are needed, notably in the framework of three-dimensional limited area simulations of a field campaign case studies including both observations and LES or CRM simulations. In such experimental conditions, it is possible to carefully assess the time evolution of the three-dimensional diabatic tendencies, using possibly different space-time resolutions. Already some improvements have recently arisen concerning the ascending convective profile in the overshoot region. Instead of considering the traditional entrainment plus moist adiabat processes, giving rise to exaggerated low temperature and consequently convective cooling, convective thermodynamical variables are taken at their buoyancy equilibrium state in this specific region of large interaction between convection and its environment. Furthermore, other new elements distinct from the convection scheme itself have improved the climate response of the model. For instance, other choices in the dynamics (Lagragian interpolation) and a more recent version of the ocean model with a larger vertical resolution have provided a reduced bias already seen in the mean climate. In a near future, additional work is planned to tighten the interactions of the convection scheme to other parametrisations. Interactions of PCMT with turbulence and non-orographic gravity wave drag are notably envisaged, directly taking into account the convective fluxes.

Acknowledgments

The authors are grateful to other people from CNRM/GMGEC and CNRM/GMAP (notably Pascal Marquet, Antoinette Alias and Michel Déqué) for their valuable help and discussions throughout the years of development and evaluation.

References

Arakawa A. 2004. The cumulus parameterization problem: Past, present and future. *J. Clim.* **17**: 2493–2525, doi: 10.1175/1520-0442(2004)017<2493:RATCPP>2.0.CO;2.

Barston AG, Livezey RE. 1987. Classification, Seasonality and Persistence of Low-Frequency Atmospheric Circulation Patterns. *Mon. Weather Rev.* **115**: 1083–1126, doi: 10.1175/1520-0493(1987)115<1083:CSAPOL>2.0.CO;2.

Bechtold P, Redelsperger JL, Beau I, Blackburn M, Brinkop S, Grandpeix JY, Grant A, Gregory D, Guichard F, Hoff C, Ioannidou E. 2000. A GCSS model intercomparison for a tropical squall line observed during TOGA-COARE. II: Intercomparison of single-column models and a cloud-resolving model. *Q. J. R. Meteorol. Soc.* **126**: 865–888, doi: 10.1002/qj.49712656405.

Bechtold P, Bazile E, Guichard F, Mascart P, Richard E. 2001. A mass-flux convection scheme for regional and global models. *Q. J. R. Meteorol. Soc.* **127**: 869–886, doi: 10.1002/qj.49712757309.

Bechtold P, Köhler M, Jung T, Doblas-Reyes F, Leutbecher M, Rodwell MJ, Vitart F, Balsamo G. 2008. Advances in simulating atmospheric variability with the ECMWF model: From synoptic to decadal time-scales. *Q.J.R. Meteorol. Soc.* **134**: 1337–1351, doi:10.1002/qj.289.

Bechtold P, Semane N, Lopez P, Chaboureau J, Beljaars A, Bormann N. 2014. Representing equilibrium and nonequilibrium convection in large-scale models. *J. Atmos. Sci.* **71**:734–753, doi: 10.1175/JAS-D-13-0163.1.

Betts AK, Miller MJ. 1986. A new convective adjustment scheme. Part II: Single-column tests using GATE wave, BOMEX, ASTEX, and arctic air-mass data sets. *Q. J. R. Meteorol. Soc.* **112**: 693–709, doi: 10.1002/qj.49711247308.

Bougeault P. 1985. A simple parameterization of the large-scale effects of cumulus convection. *Mon. Weather Rev.* **113**: 2108–2121, doi: 10.1175/1520-0493(1985)113<2108:ASPOTL>2.0.CO;2.

Bretherton CS, Mc Caa JR, Grenier H. 2004. A new parameterization for shallow cumulus convection and its application to marine subtropical cloud-topped boundary layers. Part I: Description and 1D results. *Mon. Weather Rev.* **132**: 864–882, doi: 10.1175/1520-0493(2004)132<0864:ANPFSC>2.0.CO;2.

Céron J-P, Guérémy J-F. 1999. Validation of the Space-Time Variability of African Easterly Waves Simulated by the CNRM GCM. *J. Clim.* **12**: 2831–2855, doi: 10.1175/1520-0442(1999)012<2831:VOTSTV>2.0.CO;2.

Cuxart J, Bougeault P, Redelsperger J-L. 2000. A turbulence scheme allowing for mesoscale and large-eddy simulations. *Q. J. R. Meteorol. Soc.* **126**: 1–30, doi: 10.1002/qj.49712656202.

Dee DP, Uppala SM, Simmons AJ, Berrisford P, Poli P, Kobayashi S, Andrae U, Balmaseda MA, Balsamo G, Bauer P, Bechtold P, Beljaars ACM, van de Berg L, Bidlot J, Bormann N, Delsol C, Dragani R, Fuentes M, Geer AJ, Haimberger L, Healy SB, Hersbach H, Hólm EV, Isaksen L, Kållberg P, Köhler M, Matricardi M, McNally AP, Monge-Sanz BM, Morcrette J-J, Park B-K, Peubey C, de Rosnay P, Tavolato C, Thépaut J-N, Vitart F. 2011. The ERA-Interim reanalysis: configuration and performance of the data assimilation system. *Q. J. R. Meteorol. Soc.* **137**: 553–597, doi: 10.1002/qj.828.

Derbyshire SH, Beau I, Bechtold P, Grandpeix J-Y, Piriou J-M, Redelsperger J-L, Soares, PMM. 2004. Sensitivity of moist convection to environmental humidity. *Q.J.R. Meteorol. Soc.* **130**: 3055–3079, doi: 10.1256/qj.03.130.

Duynkerke PG, de Roode SR, van Zanten MC, Calvo J, Cuxart J, Cheinet S, Chlond A, Grenier H, Jonker PJ, Köhler M, Lenderink G, Lewellen D, Lappen C-L., Lock AP, Moeng C-H, Müller F, Olmeda D, Piriou J-M, Sánchez E, Sednev I. 2004. Observations and numerical simulations of the diurnal cycle of the EUROCS stratocumulus case. *Q.J.R. Meteorol. Soc.* **130**: 3269–3296, doi: 10.1256/qj.03.139.

Emanuel KA. 1991. A scheme for representing cumulus convection in large-scale models. *J. Atmos. Sci.* **48**: 2313-2335, doi: 10.1175/1520-0469(1991)048<2313:ASFRCC>2.0.CO;2.

Gill A.E. 1980. Some simple solutions for heat-induced tropical circulation. *Q. J. R. Meteorol. Soc.* **106**: 447–462, doi: 10.1002/qj.49710644905.

Grabowski W, Kershaw R. 2004. Editorial of EUROCS Special Issue. *Q. J. R. Meteorol. Soc.* **130**: 3054, doi: 10.1256/qj.edit.1004.

Gregory D, Rowntree PR. 1990. A mass flux convection scheme with representation of cloud ensemble characteristics and stability-dependent closure. *Mon. Weather Rev.* **118**: 1483–1506, doi: 10.1175/1520-0493(1990)118<1483:AMFCSW>2.0.CO;2.

Grenier H, Bretherton CS. 2001: A moist PBL parameterization for large-scale models and its application to subtropical cloud-topped marine boundary layers. *Mon. Weather Rev.*, **129**: 357–377, doi: 10.1175/1520-0493(2001)129<0357:AMPPFL>2.0.CO;2.

Guérémy J-F. 2005. *`A buoyancy based convection and diffusion-cloud schemes.I: Description of the schemes`*, Note de Centre n°98, 20pp. Centre National de Recherches Météorologiques: Toulouse, France.

Guérémy J-F. 2011. A continuous buoyancy based convection scheme: one- and three-dimensional validation. *Tellus A* **63**: 687–706, doi: 10.1111/j.1600-0870.2011.00521.x.

Guichard F, Petch JC, Redelsperger J-L, Bechtold P, Chaboureau J-P, Cheinet S, Grabowski W, Grenier H, Jones CG, Koehler M, Piriou J-M, Tailleux R, Tomasini M. 2004. Modelling the diurnal cycle of deep precipitating convection over land with cloud-resolving models and single-column models. *Q. J. R. Meteorol. Soc.* **130**: 3139–3172 doi: 10.1256/qj.03.145.

Holland JZ, Rasmusson EM. 1973. Measurement of the atmospheric mass, energy, and momentum budgets over a 500-kilometer square of tropical ocean. *Mon. Weather Rev.* **101**: 44–55, doi: 10.1175/1520-0493(1973)101<0044:MOTAME>2.3.CO;2.

Huffman GJ, Adler RF, Morrissey MM, Bolvin DT, Curtis S, Joyce R, McGavock B, Susskind J. 2001. Global precipitation at one-degree daily resolution from multisatellite observations. *J. Hydrometeorol.* **2**: 36–50, doi: 10.1175/1525-7541(2001)002<0036:GPAODD>2.0.CO;2.

Huffman GJ, Bolvin DT, Nelkin EJ, Wolff DB, Adler RF, Gu G, Hong Y, Bowman KP, Stocker EF. 2007. The TRMM Multi-satellite Precipitation Analysis: Quasi-Global, Multi-Year, Combined-Sensor Precipitation Estimates at Fine Scale. *J. Hydrometeorol.* **8**: 38–55, doi: 10.1175/JHM560.1.

Hung M, Lin J, Wang W, Kim D, Shinoda T, Weaver SJ. 2013. MJO and Convectively Coupled Equatorial Waves Simulated by CMIP5 Climate Models. *J. Clim.* **26**: 6185–6214, doi: 10.1175/JCLI-D-12-00541.1.

Kain JS, Fritsch, JM. 1990. A one-dimensional entraining/detraining plume model and its application in convective parameterizations. *J. Atmos. Sci.* **47**: 2784–2802, doi: 10.1175/1520-0469(1990)047<2784:AODEPM>2.0.CO;2.

Klingaman NP, Jiang X, Xavier PK, Petch J, Waliser D, Woolnough SJ .2015. Vertical structure and physical processes of the Madden-Julian oscillation: Synthesis and summary. *J. Geophys. Res.* **120**: 4671–4689, doi: 10.1002/2015JD023196.

Leger J, supervised by Guérémy J-F, Beau I, Pollack D. 2015. `*Evaluation des paramétrisations physiques dans des simulations ALADIN de MCS tropicaux observés pendant la campagne AMMA*`, Rapport de stage de fin d'étude n°1330, 94pp. Ecole Nationale de la Météorologie: Toulouse, France.

Liebmann B, Smith CA. 1996. Description of a Complete (Interpolated) Outgoing Longwave Radiation Dataset. *Bull. Amer. Met. Soc.* **77**: 1275–1277.

Lopez P. 2002. Implementation and validation of a new prognostic large-scale cloud and precipitation scheme for climate and data-assimilation purposes. *Q. J. R. Meteorol. Soc.* **128**: 229–257, doi: 10.1256/00359000260498879.

Madec, G. 2008. *`NEMO reference manual, ocean dynamics component: NEMO-OPA preliminary version`*. Note du Pôle de modélisation n°27. Institut Pierre-Simon Laplace: Paris, France.

Piriou J-M., Redelsperger J-L, Geleyn J-F, Lafore J-P, Guichard F. 2007. An Approach for Convective Parameterization with Memory: Separating Microphysics and Transport in Grid-Scale Equations. *J. Atmos. Sci.* **64**: 4127–4139, doi: 10.1175/2007JAS2144.1.

Siebesma AP, Bretherton CS, Brown A, Chlond A, Cuxart J, Duynkerke PG, Jiang H, Khairoutdinov M, Lewellen D, Moeng CH, Sanchez E, Stevens B, Stevens DE. 2003. A large eddy simulation intercomparison study of shallow cumulus convection. *J. Atmos. Sci.* **60**: 1201–1219, doi: 10.1175/1520-0469(2003)60<1201:ALESIS>2.0.CO;2.

Sommeria G, Deardorff JW. 1977. Subgrid scale condensation in models of nonprecipitating clouds. *J. Atmos. Sci.* **33**: 344–355, doi: 10.1175/1520-0469(1977)034<0344:SSCIMO>2.0.CO;2.

Takayabu Y, Kimoto M. 2008. Diurnal march of rainfall simulated in a T106 AGCM and dependence on cumulus schemes. *J. Meteor. Soc. Japan* **86A**: 163–173, doi: 10.2151/jmsj.86A.163.

Tiedtke M. 1989. A comprehensive mass flux scheme for cumulus parameterization in large-scale models. *Mon. Weather Rev.* **117**: 1779–1800, doi: 10.1175/1520-0493(1989)117<1779:ACMFSF>2.0.CO;2.

Voldoire A, Sanchez-Gomez E, Salas y Mélia D, Decharme B, Cassou C, Sénési S, Valcke S, Beau I, Alias A, Chevallier M, et al. 2013. The CNRM-CM5. 1 global climate model: description and basic evaluation. *Clim. Dyn.* **40**: 2091–2121, doi: 10.1007/s00382-011-1259-y.

Wang Y, Zhou L, Hamilton K. 2007. Effect of Convective Entrainment/Detrainment on the Simulation of the Tropical Precipitation Diurnal Cycle. *Mon. Weather Rev.* **135**: 567–585, doi: 10.1175/MWR3308.1.

Wheeler M, Kiladis GN. 1999. Convectively Coupled Equatorial Waves: Analysis of Clouds and Temperature in the Wavenumber–Frequency Domain. *J. Atmos. Sci.* **56**: 374–399, doi: 10.1175/1520-0469(1999)056<0374:CCEWAO>2.0.CO;2.

Wild M, Folini D, Schär C, Loeb N, Dutton EG, König-Langlo G. 2013. The global energy balance from a surface perspective. *Clim. Dyn.* **40**: 3107–3134, doi: 10.1007/s00382-012-1569-8.

Zhang GJ, McFarlane NA. 1995. Sensitivity of climate simulations to the parameterization of cumulus convection in the Canadian Center general circulation model. *Atmos-Ocean*, **33**: 407-446, doi: 10.1080/07055900.1995.9649539.